

Numerical Solution for Nonlinear 4D Variational Data Assimilation (4D-Var) via ADMM

Bowen Li^{1,2} and Bin Shi*^{1,2}

¹State Key Laboratory of Scientific and Engineering Computing, Academy of Mathematics and Systems Science, Chinese Academy of Sciences, Beijing 100190, China

²School of Mathematical Sciences, University of Chinese Academy of Sciences, Beijing 100049, China

October 8, 2024

Abstract

The four-dimensional variational data assimilation (4D-Var) has emerged as an important methodology, widely used in numerical weather prediction, oceanographic modeling, and climate forecasting. Classical unconstrained gradient-based algorithms often struggle with local minima, making their numerical performance highly sensitive to the initial guess. In this study, we exploit the separable structure of the 4D-Var problem to propose a practical variant of the alternating direction method of multipliers (ADMM), referred to as the linearized multi-block ADMM with regularization. Unlike classical first-order optimization methods that primarily focus on initial conditions, our approach derives the Euler-Lagrange equation for the entire dynamical system, enabling more comprehensive and effective utilization of observational data. When the initial condition is poorly chosen, the argmin operation steers the iteration towards the observational data, thereby reducing sensitivity to the initial guess. The quadratic subproblems further simplify the solution process, while the parallel structure enhances computational efficiency, especially when utilizing modern hardware. To validate our approach, we demonstrate its superior performance using the Lorenz system, even in the presence of noisy observational data. Furthermore, we showcase the effectiveness of the linearized multi-block ADMM with regularization in solving the 4D-Var problems for the viscous Burgers' equation, across various numerical schemes, including finite difference, finite element, and spectral methods. Finally, we illustrate the recovery of dynamics under noisy observational data in a 2D turbulence scenario, particularly focusing on vorticity concentration, highlighting the robustness of our algorithm in handling complex physical phenomena.

1 Introduction

Data assimilation is a methodology used to estimate the evolving state of a dynamical system by integrating observational data with the system's underlying dynamics. By leveraging both sources, it produces more accurate state estimates than relying solely on either observations or

*Corresponding author: shibin@lsec.cc.ac.cn

model predictions [Asch et al., 2016]. Unlike approaches such as machine learning, image analysis, or statistical methods, data assimilation is fundamentally anchored in the dynamics of the system under study. As a result, it has emerged as a prominent research area in mathematics [Law et al., 2015, Sanz-Alonso et al., 2023]. A key application of data assimilation lies in determining initial conditions, where distributed observations collected over time are combined with the dynamic model, which significantly enhances forecast accuracy [Kalnay, 2002]. This methodology has found widespread applications across various scientific fields, including meteorology [Bouttier and Courtier, 2002], oceanography [Munk and Wunsch, 1982, Wunsch, 1996], and climatology [Siedler et al., 2013, Wunsch and Heimbach, 2013, Stammer et al., 2016].

The application of the calculus of variations to data assimilation was first pioneered by Sasaki [1958] for meteorological analysis, with subsequent extensions that incorporated the time dimension [Sasaki, 1969, 1970, Thompson, 1969]. These advancements laid the groundwork for what is now known as *4D Variational Data Assimilation*, commonly referred to as **4D-Var**. The introduction of the adjoint method by Lions [1971] and Marchuk [1975a,b] provided an efficient framework for obtaining gradient information, enabling the use of classical first-order optimization algorithms to solve these types of problems. The adoption of **4D-Var** in meteorological data assimilation gained significant momentum during the 1980s, with its theoretical foundations established by Le Dimet and Talagrand [1986] and Talagrand and Courtier [1987].

Consider a finite-dimensional dynamical system described by:

$$\begin{cases} \mathbf{u}_t = G(\mathbf{u}) \\ \mathbf{u}|_{t=0} = \mathbf{u}_0, \end{cases} \quad (1.1)$$

which $\mathbf{u} = (u_1, u_2, \dots, u_m)^\top \in \mathbb{R}^m$ is an m -dimensional vector, and its Euclidean norm is defined as:

$$\|\mathbf{u}\| = \left(\sum_{i=1}^m |u_i|^2 \right)^{\frac{1}{2}}. \quad (1.2)$$

Let $\hat{\mathbf{u}}$ represent the (partial) observational data collected over time, with indices chosen from a subset $\mathcal{S} \subseteq \{1, 2, \dots, m\}$. Additionally, let $\hat{\mathbf{u}}_0^b$ denote the data obtained from a prior prediction. The **4D-Var** problem can be rigorously formulated in the following variational form:

$$\begin{cases} \min F(\mathbf{u}) := \frac{1}{2} \int_0^T \|\mathbf{u} - \hat{\mathbf{u}}\|^2 dt + \frac{\alpha}{2} \|\mathbf{u}_0 - \hat{\mathbf{u}}_0^b\|^2 \\ \text{s.t. } \mathbf{u} \text{ satisfies (1.1),} \end{cases} \quad (1.3)$$

where $\alpha > 0$ is a regularization coefficient. In practice, observational data are typically collected at discrete time points. For simplicity, assume that observation times are uniformly spaced with $T_o = T/n$, meaning that the data is recorded at times $t = kT_o$ for $k = 0, 1, \dots, n$. Let $\mathbf{u}_k = \mathbf{u}(kT_o)$ represent the solution at time $t = kT_o$. The dynamical system (1.1) can then be expressed at these observation times as:

$$\mathbf{u}_{k+1} = H_{T_o}(\mathbf{u}_k), \quad k = 0, 1, \dots, n-1, \quad (1.4)$$

where H_{T_o} is an operator acting over the observational time interval T_o , which may be linear or nonlinear, and \mathbf{u}_0 is the given initial condition. Consequently, the continuous **4D-Var** problem (1.3)

is transformed into the following discrete form:

$$\begin{cases} \min F(\mathbf{u}_0, \mathbf{u}_1, \dots, \mathbf{u}_n) := \frac{T_o}{2} \sum_{k=0}^n \|\mathbf{u}_k - \hat{\mathbf{u}}_k\|^2 + \frac{\alpha}{2} \|\mathbf{u}_0 - \hat{\mathbf{u}}_0^b\|^2 \\ \text{s.t. } \mathbf{u}_{k+1} = H_{T_o}(\mathbf{u}_k), \quad \text{for } k = 0, 1, \dots, n-1. \end{cases} \quad (1.5)$$

1.1 Linear dynamical system

When the dynamical system (1.1) is linear, the update in the dynamical iteration (1.4) can be written as $H_{T_o}(\mathbf{u}_k) = L\mathbf{u}_k$, where L is a linear operator or matrix. This simplifies the discrete dynamical system (1.4) to:

$$\mathbf{u}_k = L^k \mathbf{u}_0, \quad \text{for } k = 0, 1, \dots, n, \quad (1.6)$$

where \mathbf{u}_0 is the given initial condition. In this case, the 4D-Var Problem (1.5) reduces to a function that depends solely on the initial condition \mathbf{u}_0 , rather than on all the intermediate states $\mathbf{u}_0, \mathbf{u}_1, \dots, \mathbf{u}_n$. The linear 4D-Var Problem can thus be reformulated as:

$$\min_{\mathbf{u}_0 \in \mathbb{R}^m} F(\mathbf{u}_0) = \frac{T_o}{2} \sum_{k=0}^n \|L^k \mathbf{u}_0 - \hat{\mathbf{u}}_k\|^2 + \frac{\alpha}{2} \|\mathbf{u}_0 - \hat{\mathbf{u}}_0^b\|^2. \quad (1.7)$$

This formulation shows that the linear 4D-Var Problem (1.5) is essentially a quadratic function of the initial condition \mathbf{u}_0 . To solve the linear 4D-Var problem (1.7), classical first-order optimization algorithms, such as the conjugate gradient method [Hestenes and Stiefel, 1952] and the limited-memory BFGS-B method [Byrd et al., 1995, Zhu et al., 1997], can be applied. The gradient required for these algorithms is computed as follows:

$$\nabla F(\mathbf{u}_0) = T_o \sum_{k=0}^n (L^k)^\top (L^k \mathbf{u}_0 - \hat{\mathbf{u}}_k) + \alpha (\mathbf{u}_0 - \hat{\mathbf{u}}_0^b), \quad (1.8)$$

where it can be observed that a key aspect of this gradient computation is the adjoint operator, $(L^k)^\top$. This procedure, commonly known as the adjoint method, was first introduced in Le Dimet and Talagrand [1986] and Talagrand and Courtier [1987]. When the system's dimension is too large to be stored L^k explicitly, iterative methods are typically employed to compute the adjoint operator $(L^k)^\top$, which poses significant challenges, particularly in extending the approach to nonlinear systems.

1.2 The Lorenz system — a nonlinear dynamical system

For the nonlinear dynamical system (1.1), where the operator H_{T_o} in the dynamical iteration (1.4) is nonlinear, the 4D-Var Problem (1.5) can still be reformulated in terms of the initial condition \mathbf{u}_0 as follows:

$$\min_{\mathbf{u}_0 \in \mathbb{R}^m} F(\mathbf{u}_0) = \frac{T_o}{2} \sum_{k=0}^n \|H_{T_o}^k(\mathbf{u}_0) - \hat{\mathbf{u}}_k\|^2 + \frac{\alpha}{2} \|\mathbf{u}_0 - \hat{\mathbf{u}}_0^b\|^2. \quad (1.9)$$

We can generalize the procedure from the linear case to solve the nonlinear problem. To apply first-order optimization algorithms to solve the 4D-Var problem (1.9), the gradient must be computed as follows:

$$\nabla F(\mathbf{u}_0) = T_o \sum_{k=0}^n \left(\nabla H_{T_o}^k(\mathbf{u}_0) \right)^\top \left(H_{T_o}^k(\mathbf{u}_0) - \hat{\mathbf{u}}_k \right) + \alpha (\mathbf{u}_0 - \hat{\mathbf{u}}_0^b). \quad (1.10)$$

The key difference between the linear case (1.8) and the nonlinear case (1.10) is that in the nonlinear case, the gradient involves the Jacobian of the nonlinear operator $H_{T_o}^k$, denoted as $\nabla H_{T_o}^k(\mathbf{u}_0)$. To compute this Jacobian efficiently, the adjoint method [Le Dimet and Talagrand, 1986, Talagrand and Courtier, 1987] is extended to nonlinear systems using the tangent linear system, which for the dynamical system (1.6) is given by:

$$\delta \mathbf{u}_t = \nabla G(\mathbf{u}) \cdot \delta \mathbf{u}. \quad (1.11)$$

From this tangent linear system (1.11), the Jacobian can be derived as:

$$\nabla H_{T_o}^k(\mathbf{u}_0) = \exp \left(\int_0^{kT_o} \nabla G(\mathbf{u}(\mathbf{u}_0, t)) dt \right). \quad (1.12)$$

Consider the classical Lorenz system, a well-known example of a nonlinear, aperiodic, and three-dimensional deterministic system known for its chaotic behavior, first studied by Lorenz [1963]. It is described by the following system of differential equations:

$$\begin{cases} \dot{x} = \sigma(y - x) \\ \dot{y} = x(\rho - z) - y \\ \dot{z} = xy - \beta z, \end{cases} \quad (1.13)$$

where the parameters are set to the classical values: $\sigma = 10$, $\rho = 28$ and $\beta = 8/3$. To numerically solve the Lorenz system (1.13), we employ the 4th-order Runge-Kutta method with a time step size of $\delta t = 0.01$ over a total time horizon of $T = 3$. The observational interval is set to $T_o = 0.3$. Following the precise observation strategy proposed in Talagrand and Courtier [1987], the numerical solution serves as the observational data. The observational data, denoted as $\hat{\mathbf{u}}_k = \mathbf{u}(kT_o)$ for $k = 0, 1, \dots, n = T/T_o = 10$, is generated using the 4th-order Runge-Kutta method for the Lorenz system (1.13) with the initial condition $\mathbf{u}_0 = (-0.5, 0.5, 20.5)$. In the context of the 4D-Var problem (1.5), we set the regularization parameter $\alpha = 0.1$. To illustrate the nonconvex nature of the objective function (1.9) associated with the Lorenz system (1.13), we visualize slices of the objective function along the X -, Y -, and Z -directions, as shown in Figure 1. These visualizations highlight the nonconvex landscape of the objective function, which arises from the chaotic dynamics inherent to the Lorenz system (1.13). As the system's nonlinearity and sensitivity to initial conditions increase, the optimization problem becomes significantly more challenging.

We then apply two classical first-order optimization algorithms, the nonlinear conjugate gradient methods [Hestenes and Stiefel, 1952, Fletcher and Reeves, 1964, Polak and Ribiere, 1969, Dai and Yuan, 1999] and the limited-memory BFGS-B method [Byrd et al., 1995, Zhu et al., 1997], to tackle the 4D-Var problem (1.5). For the Lorenz system (1.13), its tangent linear system is derived as:

$$\begin{pmatrix} \delta \dot{x} \\ \delta \dot{y} \\ \delta \dot{z} \end{pmatrix} = K[x, y, z] \begin{pmatrix} \delta x \\ \delta y \\ \delta z \end{pmatrix} = \begin{pmatrix} -\sigma & \sigma & 0 \\ \rho - z & -1 & -x \\ y & x & -\beta \end{pmatrix} \begin{pmatrix} \delta x \\ \delta y \\ \delta z \end{pmatrix}. \quad (1.14)$$

Utilizing the expression (4.2) along with the 4th-order Runge-Kutta iteration, we compute the Jacobian of the nonlinear operator $\nabla H_{T_o}^k(\mathbf{u}_0)$. Taking its transpose, $(\nabla H_{T_o}^k(\mathbf{u}_0))^\top$, allows us to obtain the gradient required for optimization. However, when these algorithms are applied to the objective function (1.9), both fail to converge the true solution, as demonstrated in Figure 2. This

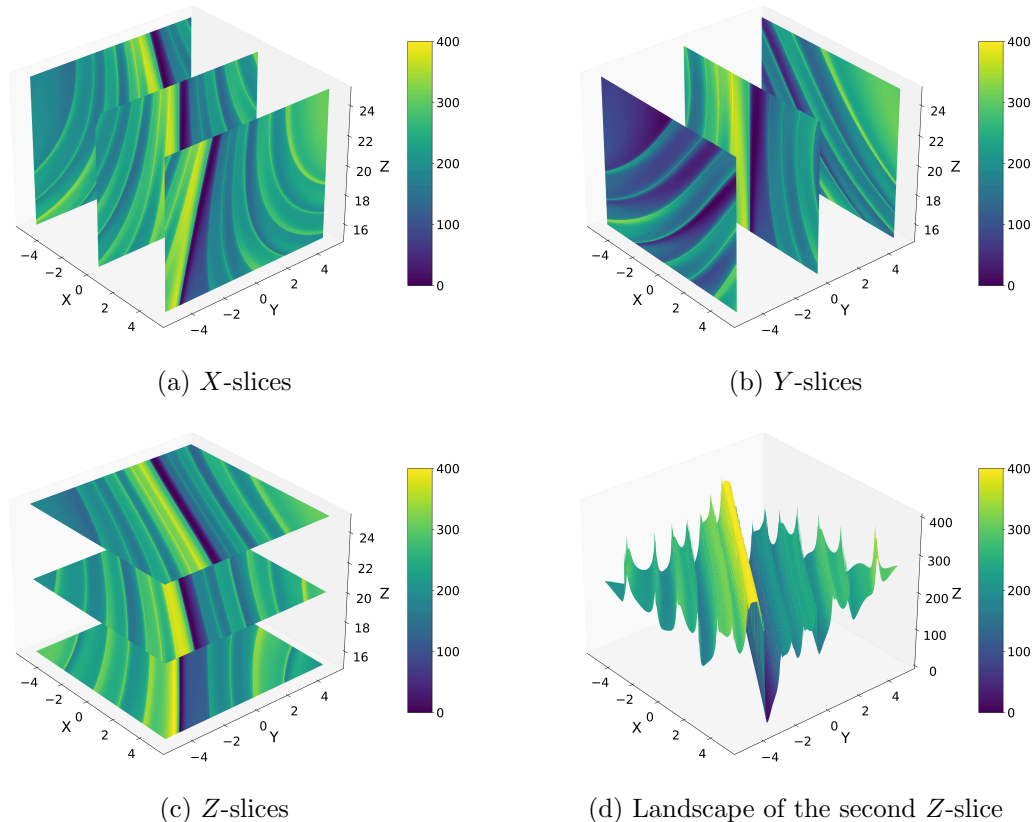


Figure 1: The objective function in (1.9) is evaluated at $\mathbf{u}_0 = (x_0, y_0, z_0) \in [-6, 6] \times [-6, 6] \times [14, 26]$ for the Lorenz system described in (1.13). In subfigures (a), (b), and (c), the colors correspond to the function values, with darker shades representing lower values and lighter shades indicating higher values.

failure is attributed to the highly nonconvex nature of the objective function, which is riddled with multiple local minima. Figure 1 illustrates the landscape of the objective function, characterized by numerous valleys and peaks. While the global minimum corresponds to the true solution, the nonconvex landscape traps both algorithms in local minima, preventing them from reaching the optimal solution. This is particularly evident in Figure 2, where the final solutions produced by both methods remain far from the global minimum. The inherent nonconvexity of the problem poses significant challenges. These classical first-order optimization methods, such as the nonlinear conjugate gradient methods and the Limited memory BFGS-B method, which are typically effective for convex problems, struggle to escape local minima. Furthermore, the nonconvex nature of the 4D-Var problem (1.9) makes the solutions obtained by these classical first-order optimization methods highly sensitive to initial conditions. This sensitivity, as noted in Talagrand [2014], is a well-known open problem that requires further in-depth investigation.

1.3 4D-Var for PDEs

In this section, we provide a brief outline of the 4D-Var problem for partial differential equations (PDEs) and its numerical implementation. Let $\Omega \subseteq \mathbb{R}^d$ be an open set with a smooth boundary

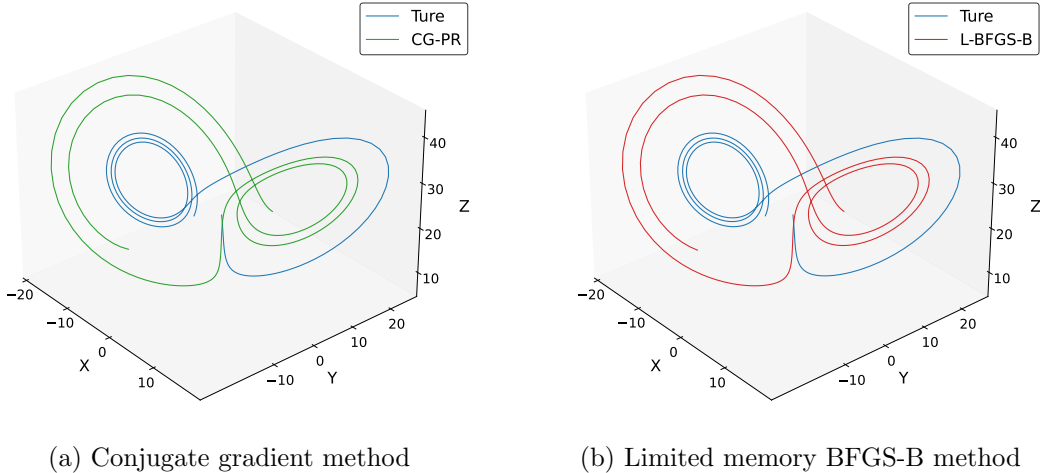


Figure 2: The optimization algorithms are applied to the 4D-Var problem (1.9) for the Lorenz system (1.13), starting with the initial condition $\mathbf{u}_0 = (x_0, y_0, z_0) = (-3, -3, 10)$. The numerical implementation is carried out using the Python subpackage — SciPy 1.14.1.

$\partial\Omega$. The general form of a PDE governing the dynamics of a system can be written as:

$$\begin{cases} u_t = G(u) \\ u|_{t=0} = u_0 \\ u|_{\partial\Omega} = g, \end{cases} \quad (1.15)$$

where $u = u(t, x)$ is a function of time $t \in (0, +\infty)$ and the spatial variable $x \in \mathbb{R}^d$, and its Energy norm, or L^2 -norm, is defined as:

$$\|u(t, \cdot)\|^2 = \int_{\Omega} |u(t, x)|^2 dx. \quad (1.16)$$

The numerical implementation of PDEs given by (1.15) often involves discretization techniques that transform the continuous system into a more tractable, finite-dimensional one. The most widely used methods include the finite difference method, finite element method, and spectral methods. While these methods differ in terms of theoretical error bounds and convergence rates, they share the goal of approximating the continuous PDE by converting it into a system of ordinary differential equations (ODEs). The solution to this discretized system, at the observational time points, can then be iteratively expressed through a discrete scheme in alignment with the observational data as outlined in (1.4).

For the 4D-Var problem, which involves data assimilation over a specific time window, the numerical implementation focuses on minimizing a cost function that quantifies the misfit between model predictions and observations, as outlined in (1.5). This minimization problem can often be reformulated as a quadratic function of the initial condition u_0 , as shown in (1.7), allowing for efficient solution of the linearized 4D-Var problem. Classical first-order optimization algorithms, such as the conjugate gradient method [Hestenes and Stiefel, 1952] and the limited-memory BFGS-B method [Byrd et al., 1995, Zhu et al., 1997], are well-suited for this task. These optimization techniques have been successfully applied to a wide range of linear PDEs, including the heat

equation [Burman and Oksanen, 2018, Li et al., 2024] and the wave equation [Burman et al., 2020].

2 Solving the 4D-Var problem via ADMM

In this section, we introduce a practical variant of the alternating direction method of multipliers (ADMM), known as multi-block ADMM, to solve the 4D-Var problem (1.5). The use of multi-block ADMM arises naturally from reformulating the 4D-Var problem (1.5) as a constraint optimization problem, which facilitates the derivation of its augmented Lagrangian. By efficiently implementing the linearized version of multi-block ADMM with regularization, we demonstrate strong numerical performance. Finally, we highlight several advantages of this approach over classical first-order unconstrained optimization algorithms, as discussed in Section 1.

2.1 Motivation and basic idea for implementing ADMM

To facilitate the integration of observational data with the system’s dynamics, it is necessary to expand the number of variables in the objective function without alternating its values. This expansion enables a more accurate representation of the system’s state over time. Given a total number of iterations $N = T/\delta t$ and $n = T_o/\delta t$ iterations per observational time interval, we increase the number of variables from n to N . This expansion allows for closer tracking of the state of the system over each discrete time step. For any $k = 0, 1, \dots, N$, the sub-objective function $f_k(\mathbf{u}_k)$ is defined as follows:

$$f_k(\mathbf{u}_k) = \begin{cases} \frac{T_o}{2} \|\mathbf{u}_0 - \hat{\mathbf{u}}_0\|^2 + \frac{\alpha}{2} \|\mathbf{u}_0 - \hat{\mathbf{u}}_0^b\|^2, & \text{for } k = 0, \\ \frac{T_o}{2} \|\mathbf{u}_{k/n} - \hat{\mathbf{u}}_{k/n}\|^2, & \text{for } k/n \in \mathbb{N}^+, \\ 0, & \text{otherwise.} \end{cases} \quad (2.1)$$

The overall 4D-Var problem (1.5) can then be reformulated as:

$$\begin{cases} \min F(\mathbf{u}_0, \mathbf{u}_1, \dots, \mathbf{u}_N) := \sum_{k=0}^N f_k(\mathbf{u}_k), \\ \text{s.t. } \mathbf{u}_{k+1} = H(\mathbf{u}_k), \quad \text{for } k = 0, 1, \dots, N-1, \end{cases} \quad (2.2)$$

where H represents the nonlinear operator that governs the evolution of the system within some numerical scheme at each time step δt .

Augmented Lagrangian Formulation Based on the constraint optimization form of the 4D-Var problem (2.2), we can then derive its augmented Lagrangian as follows:

$$\begin{aligned} L &= L(\mathbf{u}_0, \mathbf{u}_1, \dots, \mathbf{u}_N; \boldsymbol{\lambda}_0, \dots, \boldsymbol{\lambda}_{N-1}; s) \\ &= \sum_{k=0}^N f_k(\mathbf{u}_k) - \sum_{k=0}^{N-1} \langle \boldsymbol{\lambda}_k, \mathbf{u}_{k+1} - H(\mathbf{u}_k) \rangle + \frac{1}{2s} \sum_{k=0}^{N-1} \|\mathbf{u}_{k+1} - H(\mathbf{u}_k)\|^2, \end{aligned} \quad (2.3)$$

where $s > 0$ is a given parameter. By completing the square on the penalty terms, this formulation (2.3) can be simplified further:

$$L = \sum_{k=0}^N f_k(\mathbf{u}_k) + \frac{1}{2s} \sum_{k=0}^{N-1} \|\mathbf{u}_{k+1} - H(\mathbf{u}_k) - s\boldsymbol{\lambda}_k\|^2 - \frac{s}{2} \sum_{k=0}^{N-1} \|\boldsymbol{\lambda}_k\|^2. \quad (2.4)$$

From the simplified expression (2.4), we observe that \mathbf{u}_k is only related to its neighboring time steps, \mathbf{u}_{k-1} and \mathbf{u}_{k+1} , since the sub-objective function f_k depends only on \mathbf{u}_k . This local dependence simplifies the optimization process by focusing on interactions with adjacent time steps in the iterative solution.

Multi-block ADMM To demonstrate the iterative process of multi-block ADMM, we apply the arg min operation to the augmented Lagrangian during the following iteration:

$$\begin{cases} \mathbf{u}_k^{\ell+1} = \arg \min_{\mathbf{u}_k} L(\mathbf{u}_0^\ell, \dots, \mathbf{u}_{k-1}^\ell, \mathbf{u}_k, \mathbf{u}_{k+1}^\ell, \dots, \mathbf{u}_N^\ell; \boldsymbol{\lambda}_0^\ell, \dots, \boldsymbol{\lambda}_{N-1}^\ell; s), & \text{for } k = 0, \dots, N, \\ s\boldsymbol{\lambda}_k^{\ell+1} = s\boldsymbol{\lambda}_k^\ell - (\mathbf{u}_{k+1}^{\ell+1} - H(\mathbf{u}_k^{\ell+1})), & \text{for } k = 0, \dots, N-1, \end{cases} \quad (2.5)$$

where the second equation represents the update for the dual variables (Lagrange multipliers). This procedure alternates between updating the primal variables \mathbf{u}_k and the dual variables $\boldsymbol{\lambda}_k$. Substituting the simplified expression (2.4) into the arg min iteration (2.5), we can derive that the multi-block ADMM iterates as follows:

$$\begin{cases} \mathbf{u}_0^{\ell+1} = \arg \min_{\mathbf{u}_0} \left\{ f_0(\mathbf{u}_0) + \frac{1}{2s} \left\| \mathbf{u}_1^\ell - H(\mathbf{u}_0) - s\boldsymbol{\lambda}_0^\ell \right\|^2 \right\}, \\ \mathbf{u}_k^{\ell+1} = \arg \min_{\mathbf{u}_i} \left\{ f_k(\mathbf{u}_k) + \frac{1}{2s} \left\| \mathbf{u}_k - H(\mathbf{u}_{k-1}^\ell) - s\boldsymbol{\lambda}_{k-1}^\ell \right\|^2 + \frac{1}{2s} \left\| \mathbf{u}_{k+1}^\ell - H(\mathbf{u}_k) - s\boldsymbol{\lambda}_k^\ell \right\|^2 \right\}, \\ \quad \text{for } k = 1, 2, \dots, N-1, \\ \mathbf{u}_N^{\ell+1} = \arg \min_{\mathbf{u}_N} \left\{ f_N(\mathbf{u}_N) + \frac{1}{2s} \left\| \mathbf{u}_N - H(\mathbf{u}_{N-1}^\ell) - s\boldsymbol{\lambda}_{N-1}^\ell \right\|^2 \right\}, \\ s\boldsymbol{\lambda}_k^{\ell+1} = s\boldsymbol{\lambda}_k^\ell - (\mathbf{u}_{k+1}^{\ell+1} - H(\mathbf{u}_k^{\ell+1})), \quad \text{for } k = 0, 1, \dots, N-1. \end{cases} \quad (2.6)$$

In this formulation, it is observed that each block \mathbf{u}_k is updated independently, which is the key characteristic of the multi-block ADMM algorithm. While the classical two-block ADMM was originally proposed in [Glowinski and Marroco, 1975, Gabay and Mercier, 1976], the multi-block ADMM was first studied by [He et al., 2015] in the context of linear constraints. It is important to note that, even in the two-block case, the algorithm described in (2.6) may exhibit divergence, as discussed in [He et al., 2015]. The potential for divergence is a known issue in multi-block ADMM, particularly when the assumptions regarding the problem structure or linear constraints are not satisfied.

2.2 Efficient ADMM implementation

As demonstrated in [He et al., 2015], the introduction of a regularization term is a common approach to guarantee the convergence of the multi-block ADMM (2.6). Originally proposed by Zhang et al.

[2010] for the two-block case, this regularization technique is crucial for stabilizing the iterative updates and mitigating potential divergence, particularly when the underlying problem structure does not inherently guarantee convergence. Additionally, each subproblem for $k = 0, 1, \dots, N - 1$ involves solving a nonlinear least square problem, $\|\mathbf{u}_{k+1}^\ell - H(\mathbf{u}_k) - s\boldsymbol{\lambda}_k^\ell\|^2$, which incurs significant computational overhead.

Linearized multi-block ADMM with regularization To reduce computational costs and enhance efficiency, a linearization technique introduced by Deng and Yin [2016] is employed. This technique, combined with regularization, allows for a modified version of the multi-block ADMM, expressed as follows:

$$\left\{ \begin{array}{l} \mathbf{u}_0^{\ell+1} = \arg \min_{\mathbf{u}_0} \left\{ f_0(\mathbf{u}_0) - \frac{1}{s} \left\langle \nabla H(\mathbf{u}_0^\ell)^\top \left(\mathbf{u}_1^\ell - H(\mathbf{u}_0^\ell) - s\boldsymbol{\lambda}_0^\ell \right), \mathbf{u}_0 \right\rangle + \frac{\|\mathbf{u}_0 - \mathbf{u}_0^\ell\|^2}{2\eta} \right\}, \\ \mathbf{u}_k^{\ell+1} = \arg \min_{\mathbf{u}_k} \left\{ f_k(\mathbf{u}_k) + \frac{1}{2s} \left\| \mathbf{u}_k - H(\mathbf{u}_{k-1}^\ell) - s\boldsymbol{\lambda}_{k-1}^\ell \right\|^2 \right. \\ \quad \left. - \frac{1}{s} \left\langle \nabla H(\mathbf{u}_k^\ell)^\top \left(\mathbf{u}_{k+1}^\ell - H(\mathbf{u}_k^\ell) - s\boldsymbol{\lambda}_k^\ell \right), \mathbf{u}_k \right\rangle + \frac{\|\mathbf{u}_k - \mathbf{u}_k^\ell\|^2}{2\eta} \right\}, \\ \quad \text{for } k = 1, 2, \dots, N - 1, \\ \mathbf{u}_N^{\ell+1} = \arg \min_{\mathbf{u}_N} \left\{ f_N(\mathbf{u}_N) + \frac{1}{2s} \left\| \mathbf{u}_N - H(\mathbf{u}_{N-1}^\ell) - s\boldsymbol{\lambda}_{N-1}^\ell \right\|^2 + \frac{\|\mathbf{u}_N - \mathbf{u}_N^\ell\|^2}{2\eta} \right\}, \\ s\boldsymbol{\lambda}_k^{\ell+1} = s\boldsymbol{\lambda}_k^\ell - \left(\mathbf{u}_{k+1}^{\ell+1} - H(\mathbf{u}_k^{\ell+1}) \right), \quad \text{for } k = 0, \dots, n - 1, \end{array} \right. \quad (2.7)$$

where $\eta > 0$ is a regularization parameter that helps control the deviation between successive iterations. In this formulation (2.7), the linearization involves computing the gradient, which can still be efficiently obtained using the adjoint method [Le Dimet and Talagrand, 1986, Talagrand and Courtier, 1987]. The regularization term ensures that successive iterations do not deviate too far from one another, stabilizing the updates and preventing large, destabilizing steps. Thus, the linearization serves as an effective approximation for the nonlinear least square problem. Recently, several studies, including Xie and Wright [2021], El Bourkhissi et al. [2023], and Hien and Papadimitriou [2024], have explored the convergence properties of the linearized multi-block ADMM with regularization (2.7). The convergence analysis of this method has emerged as a compelling area of research.

2.3 Numerical Performance

To demonstrate the high numerical efficiency of the linearized multi-block ADMM with regularization (2.7), we use the Lorenz system (1.13) as a benchmark for comparison with the classical first-order optimization algorithms, as outlined in Section 1. The numerical solution is obtained using the 4th-order Runge-Kutta method with a time step size of $\delta t = 0.01$ over a total time horizon of $T = 3$. The observational interval is set to $T_o = 0.3$, leading to a total number of $N = T/\delta t = 300$ iterations, with $n = T/T_o + 1 = 11$ observational time points. We present

the numerical performance of the linearized multi-block ADMM with regularization (2.7) applied to the 4D-Var problem (1.5) under both precise and noisy observation conditions, highlighting its effectiveness across varying scenarios.

Precise observation The precise observational data, $(\hat{x}_1(k), \hat{y}_1(k), \hat{z}_1(k))$ for $k = 0, 1, \dots, n = 10$, is generated using the numerical solution from the 4th-order Runge-Kutta method, recorded at kT_o . To solve the 4D-Var problem (1.5), we apply the linearized multi-block ADMM with regularization (2.7), with the parameters set as $\mu = 100$, $\eta = 0.1$, and $s = 2/3$. As outlined in Section 1, the classical first-order optimization algorithms begin with the initial condition $\mathbf{u}_0 = (x_0, y_0, z_0) = (-3, -3, 10)$. To ensure consistency in comparison, the linearized multi-block ADMM with regularization (2.7) also starts with the numerical solution recorded at kT_o for $k = 0, 1, \dots, n = 10$, which is obtained using the 4th-order Runge-Kutta method under the same initial condition. The numerical performance is illustrated in Figure 3. Unlike the classical first-

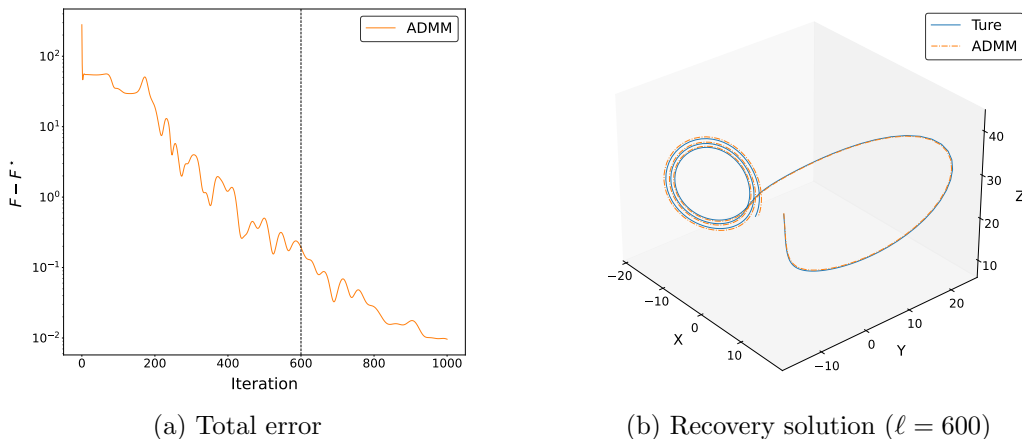


Figure 3: Numerical performance of the linearized multi-block ADMM with regularization (2.7), which is applied to the 4D-Var problem (1.9) for the Lorenz system (1.13) under the same settings as depicted in Figure 2.

order optimization algorithms, such as the nonlinear conjugate gradient method and the Limited memory BFGS-B method, which are prone to get trapped in local minima (see Figure 2), the linearized multi-block ADMM with regularization (2.7) exhibits robust convergence. It consistently reaches the true solution, as evidenced by the numerical performance shown in Figure 3.

Noisy observation The noisy observational data is generated by adding Gaussian noise to the precise observational data. Specifically, the noisy data is given by:

$$(\hat{x}_2(k), \hat{y}_2(k), \hat{z}_2(k)) = (\hat{x}_1(k) + \varepsilon_1, \hat{y}_1(k) + \varepsilon_2, \hat{z}_1(k) + \varepsilon_3), \quad (2.8)$$

where $\varepsilon_i \sim \mathcal{N}(0, 1)$ for any $i = 1, 2, 3$. Under the same settings as in the precise observation case, we apply the linearized multi-block ADMM with regularization (2.7) to solve the 4D-Var problem (1.5). The resulting numerical performance is depicted in Figure 4. By comparing Figure 3a (precise observation) and Figure 4a (noisy observation), we observe a key difference: in the precise observation scenario, the total error converges consistently to zero, while in the noisy observation scenario, the total error converges to a non-zero value due to the influence of the noise.

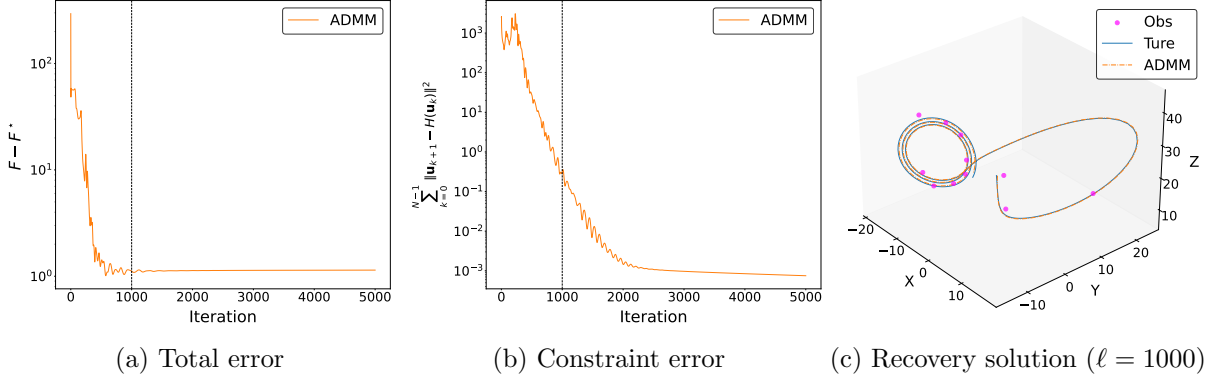


Figure 4: Numerical performance of the linearized multi-block ADMM with regularization (2.7), which is applied to the 4D-Var problem (2.2) for the Lorenz system (1.13) under noisy observation conditions, as specified in (2.8).

However, despite this noise-induced offset, the convergence remains stable, indicating robustness in the optimization process. Moreover, as illustrated in Figure 4b, we continue to monitor the constraint, $\sum_{k=0}^{N-1} \|\mathbf{u}_{k+1} - H(\mathbf{u}_k)\|^2$, which ensures that the solution recovered by the linearized multi-block ADMM with regularization (2.7) remains accurate. Finally, Figure 4c shows that, despite the presence of noise, the recovered solution remains close to the true numerical solution, demonstrating the method’s resilience in handling noisy data while maintaining a high degree of accuracy.

2.4 Advantages of the linearized multi-block ADMM with regularization

The algorithmic structure of the linearized multi-block ADMM with regularization (2.7), along with its numerical performance as demonstrated in Figure 3 and Figure 4, highlights several significant advantages for solving the 4D-Var problem (1.5). These advantages are outlined as follows:

- (1) **Effective Utilization of Observational Data** In solving the 4D-Var problem with classical first-order optimization algorithms, the solution is assumed to strictly follow the governing dynamics, making it highly sensitive to the selection of initial conditions. This sensitivity, combined with noise in observational data, can significantly degrade performance. However, when using the linearized multi-block ADMM with regularization (2.7), the recovered solution captures the whole dynamics, not just the initial condition. At the outset, the iterative points do not need to strictly satisfy the constraints, or be a specific dynamical solution; they only need to converge toward the constraints. Particularly in the early stages, if the initial condition is far from the observational data, the arg min operation effectively pulls the solution closer to the data without being constrained to a specific dynamical solution. Additionally, a scaling parameter $\mu > 0$ can be introduced in the objective function to balance the solution between the observational data and constraints, improving overall performance.
- (2) **Quadratic Subproblems** In the linearized multi-block ADMM with regularization (2.7), each subproblem is framed as a quadratic function, simplifying the optimization process. By adjusting the regularization coefficient $\eta > 0$, the difference between consecutive iterations $\mathbf{u}^{\ell+1}$ and \mathbf{u}^{ℓ} becomes smaller, making the linearization a reasonable approximation. The

flexibility in tuning the parameters $\mu > 0$ and $\eta > 0$ allows us to improve the optimization performance. However, as the time step size δt increases, the nonlinearity in the updates becomes more pronounced, which can degrade its performance.

- (3) **Parallelizable Implementation** The linearized multi-block ADMM with regularization (2.7) is well-suited for parallel implementation. This feature is especially advantageous for problems involving long-term nonlinear evolutions, where computational demands can be substantial. With sufficient computing resources, the method can be implemented effectively, making it scalable and practical for real-world applications.

Overall, these advantages highlight the efficiency and practical utility of the linearized multi-block ADMM with regularization (2.7) in addressing the complex 4D-Var problem (1.5).

3 Viscous Burgers' equation

In this section, we apply the 4D-Var problem (1.5) to a classical nonlinear PDE — the viscous Burgers' equation. The solution is assumed to satisfy $u \in L^2([0, T]; H_0^1([0, \pi]))$ and $u_t \in L^2([0, T]; H^{-1}([0, \pi]))$. Under the Dirichlet boundary condition, the viscous Burgers' equation is given by:

$$\begin{cases} \partial_t u + u \cdot \partial_x u = \gamma \partial_{xx} u \\ u(0, x) = \sin x \\ u(t, 0) = u(t, \pi) = 0, \end{cases} \quad (3.1)$$

where the viscous coefficient is $\gamma = 0.05$. We demonstrate the numerical performance of the linearized multi-block ADMM with regularization (2.7), based on the 4D-Var reformulation (2.2), across various numerical discretization methods, including finite difference, (Galerkin) finite element, and spectral methods. For time discretization, we employ the forward Euler scheme.

3.1 Finite difference method

Let the time step size be $\delta t = 0.02$ and the total evolution time $T = 2$. The spatial grid size is set to $m = 100$, resulting in a spatial discretization of $\delta x = \pi/m$. The spatial grid points x_i , for $i = 0, \dots, m$, are illustrated in Figure 5. For spatial discretization, we apply the central difference

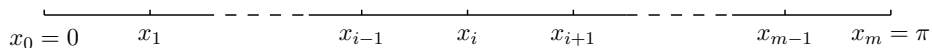


Figure 5: Uniform spatial discretization of the interval $[0, \pi]$.

scheme. Given the Dirichlet boundary condition, $u(t, 0) = u(t, \pi) = 0$, we focus on the interior spatial grid points x_i for $i = 1, 2, \dots, m - 1$.

For $k = 0, 1, \dots, N = T/\delta t = 100$, let $u_{k,i} = u_{k,i}^{(m)}$ represent the finite difference approximation of the analytic solution $u(k\delta t, i\delta x)$. For the viscous Burgers' equation (3.1), the central difference scheme is given by:

$$\frac{u_{k+1,i} - u_{k,i}}{\delta t} + \frac{(u_{k,i+1})^2 - (u_{k,i-1})^2}{4\delta x} = \gamma \cdot \frac{u_{k,i+1} + u_{k,i-1} - 2u_{k,i}}{(\delta x)^2}. \quad (3.2)$$

This scheme (3.2) can be reformulated into the iterative update form $\mathbf{u}_{k+1} = H(\mathbf{u}_k)$, as follows:

$$u_{k+1,i} = \left[\frac{\gamma\delta t}{(\delta x)^2} \cdot u_{k,i-1} + \frac{\delta t}{4\delta x} \cdot (u_{k,i-1})^2 \right] + \left(1 - \frac{2\gamma\delta t}{(\delta x)^2} \right) u_{k,i} + \left[\frac{\gamma\delta t}{(\delta x)^2} \cdot u_{k,i+1} - \frac{\delta t}{4\delta x} \cdot (u_{k,i+1})^2 \right], \quad (3.3)$$

for $i = 1, 2, \dots, m-1$. Let the observational time be $T_o = 0.2$, resulting in $n+1$ observational time points, where $n = T/T_o = 10$. The numerical solution is generated using the central difference scheme (3.2), with the initial condition $u_{0,i} = \sin(i\pi/m)$ for $i = 1, 2, \dots, m-1$. The precise observational data is recorded at intervals of T_o , corresponding to the numerical solution \mathbf{u}_{10k} for $i = 0, 1, \dots, n$, where each component is $u_{10k,i}$ for $i = 1, 2, \dots, m-1$. Gaussian noise is then added to the precise observations to produce noisy observational data $\hat{\mathbf{u}}_k$, given by:

$$\hat{u}_{k,i} = u_{10k,i} + 0.1\varepsilon_i \quad (3.4)$$

where $\varepsilon_i \sim \mathcal{N}(0, 1)$ for $i = 1, 2, \dots, m-1$.

The tangent linear iteration corresponding to the iterative update (3.3) is given by:

$$\delta u_{k+1,i} = \left[\frac{\gamma\delta t}{(\delta x)^2} + \frac{\delta t}{2\delta x} \cdot u_{k,i-1} \right] \delta u_{k,i-1} + \left(1 - \frac{2\gamma\delta t}{(\delta x)^2} \right) \delta u_{k,i} + \left[\frac{\gamma\delta t}{(\delta x)^2} - \frac{\delta t}{2\delta x} \cdot u_{k,i+1} \right] \delta u_{k,i+1}, \quad (3.5)$$

for $i = 1, 2, \dots, m-1$, which allows us to compute the Jacobian matrix, $\nabla H(\mathbf{u}_k)$. Since $m = 99$ is not large, its adjoint operator, $\nabla H(\mathbf{u}_k)^\top$, is easily obtained. The linearized multi-block ADMM with regularization (2.7) is then applied to solve the 4D-Var problem (2.2). The initial condition is set as $\mathbf{u}_k^0 = (0, 0, \dots, 0)^\top$ for $k = 0, 1, \dots, N$, with parameters $\mu = 20$, $\eta = 0.1$, and $s = 2/3$.

Figure 6 illustrates the numerical performance, highlighting the convergence behavior of both

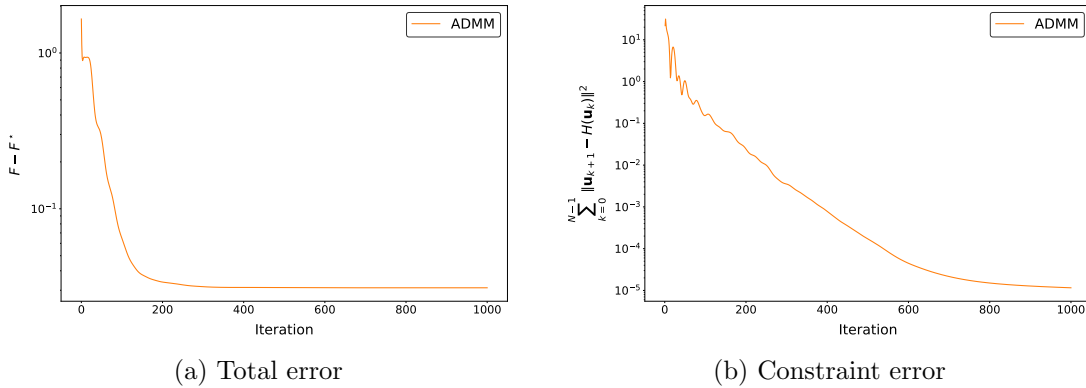


Figure 6: The linearized multi-block ADMM with regularization (2.7) is applied to the 4D-Var problem (2.2) for the viscous Burgers' equation (3.1), using the finite difference method (3.2).

the total error and the constraint error for the linearized multi-block ADMM with regularization (2.7), applied to the 4D-Var problem (2.2) for the viscous Burgers' equation using the finite difference method (3.2). The total error stabilizes while the constraint error consistently converges, exhibiting

a similar pattern to that observed in the Lorenz system (Figure 4). Additionally, Figure 7 compares the dynamical evolution recovered via the linearized multi-block ADMM with regularization (2.7) with the noisy observational data, using the true numerical solution as a reference. Despite the presence

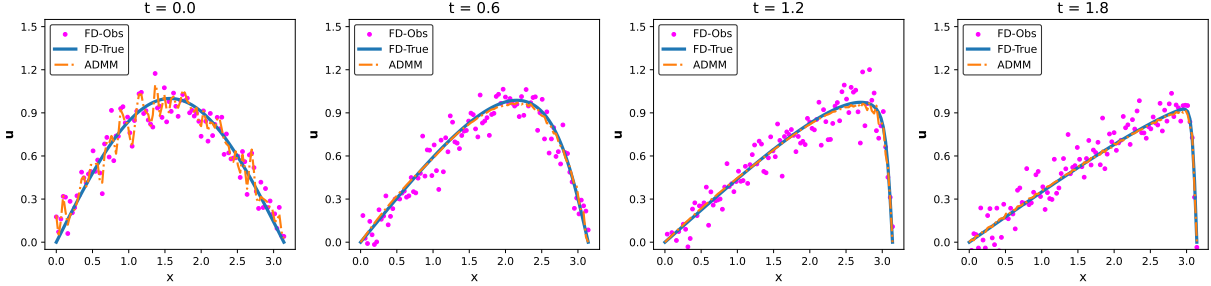


Figure 7: Comparison of noisy observational data with the time evolution dynamics recovered via the linearized multi-block ADMM with regularization (2.7), with the true numerical solution as the reference.

of noise, the recovered dynamics closely match the true numerical solution, with accuracy improving over time.

3.2 (Galerkin) Finite element method

In the finite element method, the time step size is set to $\delta t = 0.01$ with a total evolution time of $T = 2$. The spatial grid points are identical to those used in the finite difference method, as shown in Figure 5. Since the solution $u = u(t, x)$ satisfies the Dirichlet boundary condition $u(t, 0) = u(t, \pi) = 0$, the Lagrange nodal basis functions are defined as:

$$\varphi_i = \begin{cases} \frac{x - x_{i-1}}{\delta x}, & x \in [x_{i-1}, x_i] \\ \frac{x_{i+1} - x}{\delta x}, & x \in [x_i, x_{i+1}] \\ 0, & \text{otherwise} \end{cases} \quad (3.6)$$

for $i = 1, 2, \dots, m - 1$, as depicted in Figure 8.

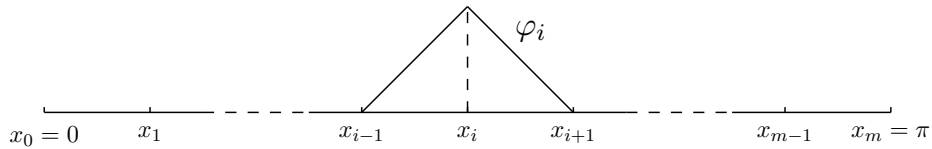


Figure 8: Uniform spatial discretization of the interval $[0, \pi]$ and Lagrange nodal basis functions φ_i for $i = 1, 2, \dots, m - 1$.

For $k = 0, 1, \dots, N = T/\delta t$ and $i = 1, 2, \dots, m - 1$, the numerical solution can be expressed as the following linear combination:

$$u_k(x) = u_k^{(m)}(x) = \sum_{i=1}^{m-1} u_{k,i} \varphi_i(x),$$

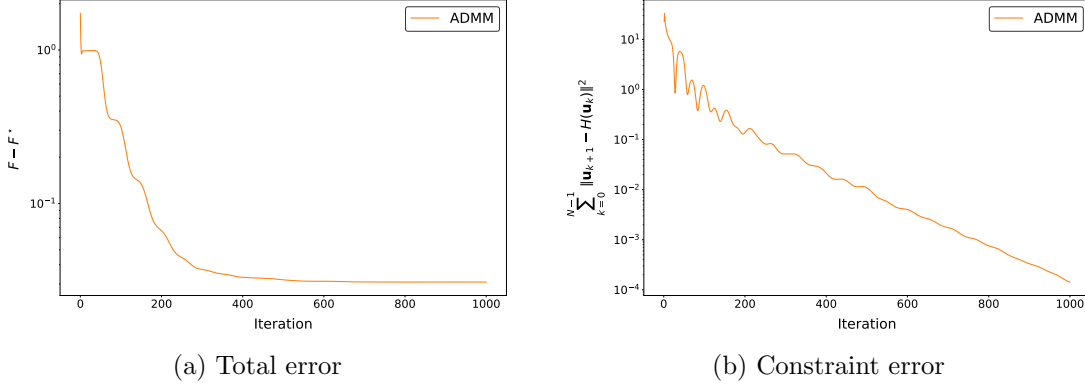


Figure 9: The linearized multi-block ADMM with regularization (2.7) is applied to the 4D-Var problem (2.2) for the viscous Burgers' equation (3.1), using the finite element method (3.7)

$\mu = 20$, $\eta = 0.1$, and $s = 2/3$. The numerical performance, displayed in Figure 9, shows convergence behaviors similar to that observed in Figure 6. As the iterations increase, the total error stabilizes, while the constraint error consistently decreases. Figure 10 demonstrates the numerical performance of the dynamics recovered via the linearized multi-block ADMM with regularization (2.7). The recovered dynamics closely track the true numerical solution, with only minor deviations due

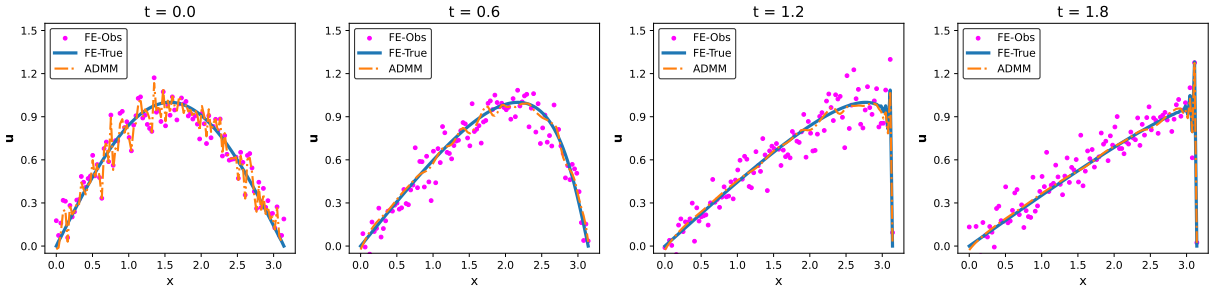


Figure 10: Comparison of noisy observational data with the time evolution dynamics recovered via the linearized multi-block ADMM with regularization (2.7), with the true numerical solution as the reference.

to noise in the observational data, and the accuracy improves over time. A key observation is that the finite difference method exhibits numerical dissipation without high-frequency oscillations, while the finite element method lacks numerical dissipation but contains high-frequency oscillations. The solution recovered via the multi-block ADMM with regularization (2.7) reflects the characteristics of the different numerical discretizations used to generate the observational data, highlighting this method's effectiveness in solving the 4D-Var problem (1.5) and its dependence on the observational data.

3.3 Spectral method

For the spectral method, we also set the time step size $\delta t = 0.01$ and the total evolution time $T = 2$. Let m be the total degrees of freedom. Given the Dirichlet boundary condition $u(t, 0) = u(t, \pi) = 0$, we select sine functions $\sin ix$ for $i = 1, 2, \dots, m$ as the orthogonal basis. For each time step

$k = 0, 1, \dots, N = T/\delta t$, the numerical solution is expressed as the following linear combination:

$$u_k(x) = u_k^{(m)}(x) = \sum_{i=1}^m u_{k,i} \sin ix,$$

which serves as the spectral approximation for the analytic solution $u(k\delta t, x)$. The vector of coefficients $\mathbf{u}_k = (u_{k,1}, u_{k,2}, \dots, u_{k,m})^\top$, satisfies the following iterative scheme:

$$\begin{cases} \frac{u_{k+1,1} - u_{k,1}}{\delta t} - \frac{1}{2} \sum_{l=1}^{m-1} u_{k,l} u_{k,l+1} = -\gamma u_{k,1}, \\ \frac{u_{k+1,i} - u_{k,i}}{\delta t} + \frac{i}{4} \left(\sum_{l=1}^i u_{k,l} u_{k,i-l} - 2 \sum_{l=1}^{m-i} u_{k,l} u_{k,i+l} \right) = -\gamma i^2 u_{k,i}, \end{cases} \quad \text{for } i = 2, 3, \dots, m. \quad (3.10)$$

The observational setup remains the same, with observational time $T_o = 0.2$ and $n + 1$ observational time points, where $n = T/T_o = 10$. The numerical solution is generated using the spectral method (3.10), starting from the initial condition $\mathbf{u}_0 = (1, 0, \dots, 0)^\top$. At each time observational point, the numerical solution \mathbf{u}_{10k} is recorded for $i = 0, 1, \dots, n$ with each component denoted as $u_{10k,i}$ for $i = 1, 2, \dots, m - 1$. Noisy observational data $\hat{\mathbf{u}}_k$ is generated by adding Gaussian noise to the observations:

$$\hat{u}_{k,i} = u_{10k,i} + 0.1\sqrt{2} \cdot 0.1\varepsilon_i \quad (3.11)$$

where $\varepsilon_i \sim \mathcal{N}(0, 1)$ for $i = 1, 2, \dots, m - 1$ and the scaling factor $0.1\sqrt{2}$ ensures consistency with previous cases.

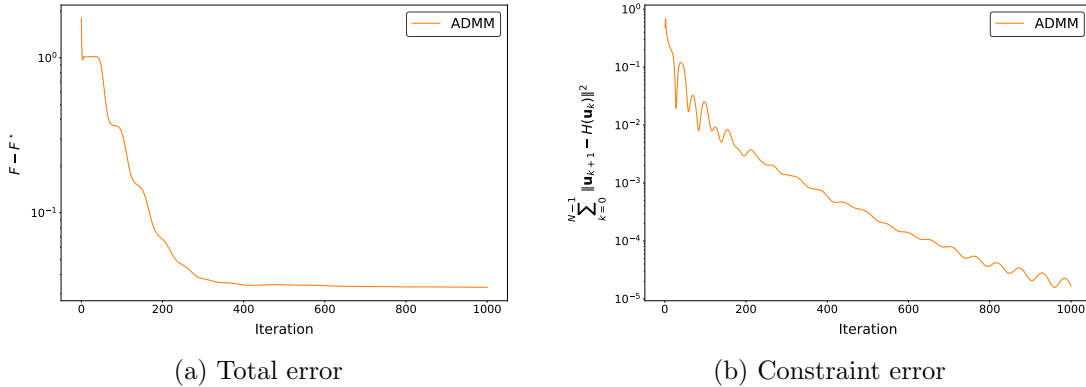


Figure 11: The linearized multi-block ADMM with regularization (2.7) is applied to the 4D-Var problem (1.9) for the viscous Burgers' equation (3.1), using the spectral method (3.10).

Before applying the linearized multi-block ADMM with regularization (2.7) to solve the 4D-Var problem (2.2), we first derive the tangent linear iteration corresponding to the iterative scheme (3.10)

as follows:

$$\begin{cases} \delta u_{k+1,1} = \delta u_{k,1} + \delta t \left(\frac{1}{2} \sum_{l=1}^{m-1} \delta u_{k,l} \cdot u_{k,l+1} + \frac{1}{2} \sum_{l=1}^{m-1} u_{k,l} \cdot \delta u_{k,l+1} - \gamma \delta u_{k,1} \right), \\ \delta u_{k+1,i} = \delta u_{k,i} - \delta t \gamma i^2 \cdot \delta u_{k,i} \\ - \delta t \cdot \frac{i}{4} \left(\sum_{l=1}^i \delta u_{k,l} \cdot u_{k,i-l} + \sum_{l=1}^i u_{k,l} \cdot \delta u_{k,i-l} - 2 \sum_{l=1}^{m-i} \delta u_{k,l} \cdot u_{k,i+l} - 2 \sum_{l=1}^{m-i} u_{k,l} \cdot \delta u_{k,i+l} \right), \\ \text{for } i = 2, 3, \dots, m, \end{cases} \quad (3.12)$$

which helps us derive the Jacobian matrix $\nabla H(\mathbf{u}_k)$ and its adjoint $\nabla H(\mathbf{u}_k)^\top$. The iterative process begins with the initial condition as $\mathbf{u}_k^0 = (0, 0, \dots, 0)^\top$ for $k = 0, 1, \dots, N$, using the parameters $\mu = 20$, $\eta = 0.1$, and $s = 2/3$. The numerical performance is illustrated in Figure 11, showing consistency with the convergence behaviors observed in Figure 6 and Figure 9. Furthermore, Figure 12 highlights the recovered dynamics, indicating that the solution recovered via the multi-block ADMM with regularization (2.7) effectively captures the characteristics of the different numerical discretizations used to generate the observational data.

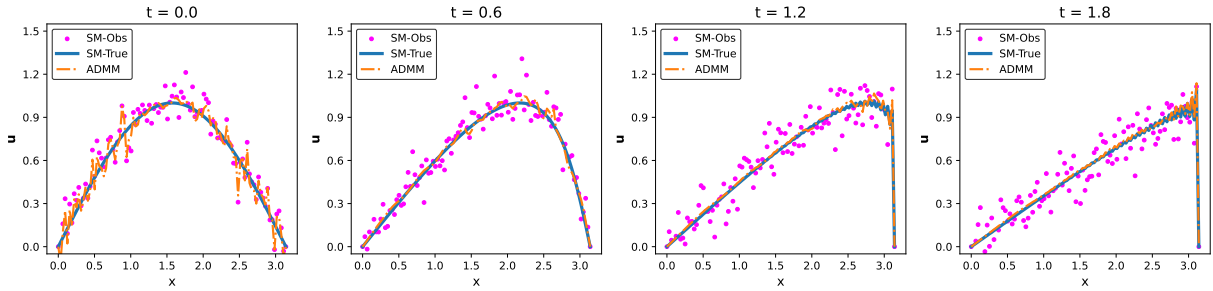


Figure 12: Comparison of noisy observational data with the time evolution dynamics recovered via the linearized multi-block ADMM with regularization (2.7), with the true numerical solution as the reference.

Finally, a comparison of the spectral method (3.10) with the finite difference method (3.2) and the finite element method (3.7) reveals key distinctions in their computational complexity. The spectral method includes $m^2 - 1$ quadratic terms in the spectral method, while the finite difference method has $2m - 2$, and the finite element method involves $6m - 10$ quadratic terms. This difference leads the tangent linear iteration (3.12) to introduce nonlinear terms that scale as $O(m^2)$ for the spectral method. As a result, the computational cost, particularly for calculating

Numerical Methods	Computational Time
Finite Difference	65.5021s
Finite Element	232.0715s
Spectral Method	5113.0345s

Table 1: Comparison of computational times for the linearized multi-block ADMM with regularization (2.7) across the finite difference (3.2), finite element (3.7), and spectral (3.10) discretizations. Python 3.11.5 and Numpy 1.25.2 were executed on an Intel® Core™ i5-12500, 3.00 GHz Processor (12th Generation).

the adjoint operator, increases significantly. This higher complexity makes the spectral method substantially slower compared to the other methods, as evidenced by the computational times presented in Table 1.

4 Vorticity concentration in large-scale 2D turbulence

In this section, we apply the linearized multi-block ADMM with regularization (2.7) to solve the 4D-Var problem (2.2) in the context of the large-scale 2D turbulence, with a particular focus on the phenomenon of vorticity concentration. Let Ω be an open domain, and the vorticity field is assumed to satisfy $\omega \in L^2([0, T]; H_0^1(\Omega))$ and $\omega_t \in L^2([0, T]; H^{-1}(\Omega))$. The governing 2D vorticity equation is given by:

$$\begin{cases} \partial_t \omega + J(\psi, \omega) = -\kappa \Delta^2 \omega, \\ \omega = \Delta \psi, \end{cases} \quad (4.1)$$

where the Jacobian J , for any bivariate functions u and v , is defined as:

$$J(u, v) = \partial_x u \partial_y v - \partial_y u \partial_x v, \quad (4.2)$$

and the biharmonic operator Δ^2 serves as a scale-selective dissipation, filtering out high-frequency waves, as described in [McWilliams, 1984]. We impose a slip boundary condition:

$$\omega|_{\partial\Omega} = 0, \quad (4.3)$$

which indicates the absence of tangential stress along the boundary for large-scale flow. Small-scale processes occurring near the boundary act as a buffer, allowing the large-scale flow to slip smoothly along the boundary. This condition is commonly used in large-scale ocean circulation models [Pedlosky, 1996, Section 2.4].

4.1 Computational Implementation

For the numerical implementation, we utilize a finite difference scheme, applying the Arakawa Jacobian, which is specifically designed to conserve energy and enstrophy in 2D fluid dynamics. In particular, we adopt the second-order Arakawa Jacobian as outlined in [Cushman-Roisin and Beckers, 2011, Section 16.7], which consists of three components:

$$\left\{ \begin{array}{l} J_1^{i,j} = \frac{(u^{i+1,j} - u^{i-1,j})(v^{i,j+1} - v^{i,j-1}) - (u^{i,j+1} - u^{i,j-1})(v^{i+1,j} - v^{i-1,j})}{4\delta x \delta y}, \\ J_2^{i,j} = \frac{u^{i+1,j}(v^{i+1,j+1} - v^{i+1,j-1}) - u^{i-1,j}(v^{i-1,j+1} - v^{i-1,j-1})}{4\delta x \delta y} \\ \quad - \frac{u^{i,j+1}(v^{i+1,j+1} - v^{i-1,j+1}) - u^{i,j-1}(v^{i+1,j-1} - v^{i-1,j-1})}{4\delta x \delta y}, \\ J_3^{i,j} = \frac{(u^{i+1,j+1} - u^{i-1,j+1})v^{i,j+1} - (u^{i+1,j-1} - u^{i-1,j-1})v^{i,j-1}}{4\delta x \delta y} \\ \quad - \frac{(u^{i+1,j+1} - u^{i+1,j-1})v^{i+1,j} - (u^{i-1,j+1} - u^{i-1,j-1})v^{i-1,j}}{4\delta x \delta y}. \end{array} \right.$$

The total Arakawa Jacobian is then computed as the average of these three components:

$$J^{i,j} = \frac{J_1^{i,j} + J_2^{i,j} + J_3^{i,j}}{3}. \quad (4.4)$$

Figure 13 illustrates the spatial grid around the central grid point (i, j) , highlighting the neighboring points used in the computation of the Jacobian. Numerically, both \mathbf{u} and \mathbf{v} are treated as vectors,

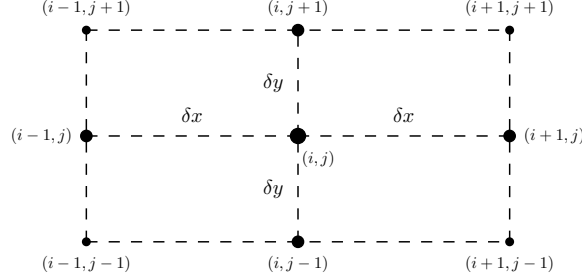


Figure 13: Spatial grids for numerical Arakawa Jacobian $J(\mathbf{u}, \mathbf{v})$ around the central point labeled (i, j) .

when substituting a variable into the Arakawa Jacobian (4.4), it acts as a linear operator on the other variable, expressed as

$$J(\mathbf{u}, \mathbf{v}) = (J^{i,j})_{m^2 \times m^2} = \mathbb{J}[\mathbf{u}]\mathbf{v} = -\mathbb{J}[\mathbf{v}]\mathbf{u}. \quad (4.5)$$

To solve the inverse Laplacian, we utilize the successive over-relaxation (SOR) method [Golub and Van Loan, 2013], though the conjugate gradient method [Hestenes and Stiefel, 1952] is also a widely used approach. For time discretization, we employ a prediction-correction scheme:

$$\begin{cases} \frac{\boldsymbol{\omega}_k^p - \boldsymbol{\omega}_k}{\delta t} + J(\boldsymbol{\psi}_k, \boldsymbol{\omega}_k) = -\kappa \Delta^2 \boldsymbol{\omega}_k, & (4.6a) \\ \frac{\boldsymbol{\omega}_{k+1} - \boldsymbol{\omega}_k}{\delta t} + J(\boldsymbol{\psi}_k, \boldsymbol{\omega}_k^p) = -\kappa \Delta^2 \boldsymbol{\omega}_k^p. & (4.6b) \end{cases}$$

which ensures both accuracy and stability. The tangent linear iterations for the prediction-correction scheme (4.6) are given by:

$$\begin{cases} \frac{\delta \boldsymbol{\omega}_k^p - \delta \boldsymbol{\omega}_k}{\delta t} - \mathbb{J}[\boldsymbol{\omega}_k] \Delta^{-1} \delta \boldsymbol{\omega}_k + \mathbb{J}[\Delta^{-1} \boldsymbol{\omega}_k] \delta \boldsymbol{\omega}_k = -\kappa \Delta^2 \delta \boldsymbol{\omega}_k, & (4.7a) \\ \frac{\delta \boldsymbol{\omega}_{k+1} - \delta \boldsymbol{\omega}_k}{\delta t} - \mathbb{J}[\boldsymbol{\omega}_k^p] \Delta^{-1} \delta \boldsymbol{\omega}_k + \mathbb{J}[\Delta^{-1} \boldsymbol{\omega}_k] \delta \boldsymbol{\omega}_k^p = -\kappa \Delta^2 \delta \boldsymbol{\omega}_k^p. & (4.7b) \end{cases}$$

Reformulating (4.6a) gives:

$$\boldsymbol{\omega}_k^p = \mathbb{P} \boldsymbol{\omega}_k = [\mathbb{I} - \delta t (\mathbb{J}[\Delta^{-1} \boldsymbol{\omega}_k] - \kappa \Delta^2)] \boldsymbol{\omega}_k, \quad (4.8)$$

and similarly, reformulating (4.7a) gives:

$$\delta \boldsymbol{\omega}_k^p = \delta \mathbb{P} \delta \boldsymbol{\omega}_k = [\mathbb{I} + \delta t (\mathbb{J}[\boldsymbol{\omega}_k] \Delta^{-1} - \mathbb{J}[\Delta^{-1} \boldsymbol{\omega}_k] - \kappa \Delta^2)] \delta \boldsymbol{\omega}_k. \quad (4.9)$$

Substituting (4.8) and (4.9) into (4.7b) allows us to derive the tangent linear iteration:

$$\delta\boldsymbol{\omega}_{k+1} = [\mathbb{I} + \delta t (\mathbb{J}[\mathbb{P}\boldsymbol{\omega}_k]\Delta^{-1} - (\mathbb{J}[\Delta^{-1}\boldsymbol{\omega}_k] + \kappa\Delta^2)\delta\mathbb{P})] \delta\boldsymbol{\omega}_k \quad (4.10)$$

and the adjoint operator of $\nabla H(\boldsymbol{\omega}_k)$ is given by:

$$\nabla H(\boldsymbol{\omega}_k)^\top = \left[\mathbb{I} + \delta t \left(\Delta^{-1}\mathbb{J}[\mathbb{P}\boldsymbol{\omega}_k]^\top - \delta\mathbb{P}^\top(\mathbb{J}[\Delta^{-1}\boldsymbol{\omega}_k]^\top + \kappa\Delta^2) \right) \right], \quad (4.11)$$

which highlights the complexity of computing the adjoint operator in this context. Before implementing the linearized multi-block ADMM with regularization (2.7) to solve the 4D-Var problem (2.2), we must establish the energy norm for the objective function as:

$$\begin{aligned} F(\boldsymbol{\omega}_0, \boldsymbol{\omega}_1, \dots, \boldsymbol{\omega}_n) &= \frac{T_o}{2} \sum_{k=0}^n \|\nabla^\top(\boldsymbol{\psi}_k - \hat{\boldsymbol{\psi}}_k)\|^2 + \frac{\alpha}{2} \|\nabla^\top(\boldsymbol{\psi}_0 - \hat{\boldsymbol{\psi}}_0^b)\|^2 \\ &= \frac{T_o}{2} \sum_{k=0}^n \|\Delta^{-\frac{1}{2}}(\boldsymbol{\omega}_k - \hat{\boldsymbol{\omega}}_k)\|^2 + \frac{\alpha}{2} \|\Delta^{-\frac{1}{2}}(\boldsymbol{\omega}_0 - \hat{\boldsymbol{\omega}}_0^b)\|^2, \end{aligned} \quad (4.12)$$

where the second equation results from integration by parts.

4.2 Numerical performance

We demonstrate the numerical performance within a box domain defined as $\Omega = [-2L, 2L] \times [-2L, 2L]$ where $L = 1$. The spatial grids are configured with $\delta x = \delta y = 0.2$, resulting in $4L/\delta x = 4L/\delta y = m = 20$ grid points along each axis. The time step size is chosen as $\delta t = 3\delta x\delta y$, and the biharmonic coefficient is specified as $\kappa = 0.001\delta x\delta y$. Notably, the equations under consideration have been nondimensionalized. With an iteration count of $N = 300$, we achieve a total simulation time $T = N\delta t = 36$. The initial condition is randomly generated as $\omega_{0;ij} \sim 5\mathcal{N}(0, 1)$ for $i, j = 1, 2, \dots, m - 1$. The numerical solution, considered as the precise observation, is obtained following

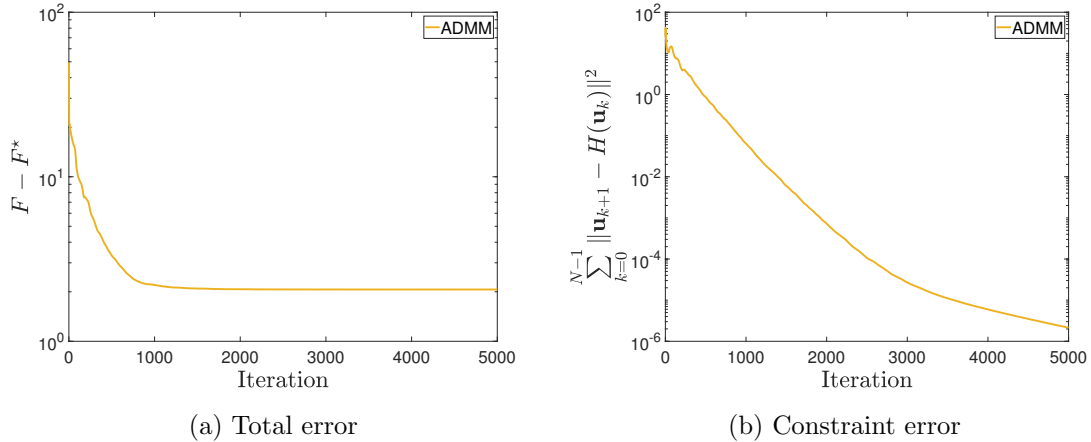


Figure 14: The linearized multi-block ADMM with regularization (2.7) is applied to the 4D-Var problem (2.2) for the Burgers' equation with the 2D large-scale vorticity equation (4.1), using the finite difference scheme described in Section 4.1.

the procedures outlined in Section 4.1, To generate noisy observational data, we add Gaussian noise to the observations: $\hat{\omega}_{k,ij} = \omega_{30k,ij} + 0.5\varepsilon_{ij}$, where $\varepsilon_{ij} \sim \mathcal{N}(0,1)$ for $i,j = 1,2,\dots,m-1$. The linearized multi-block ADMM with regularization (2.7) begins with the initial condition as $\omega_k^0 = 0_{(m-1)\times(m-1)}^\top$ for $k = 0,1,\dots,N$, using the parameters $\mu = 20$, $\eta = 0.1$, and $s = 2/3$. The numerical performance is illustrated in Figure 14, which shows consistency with the convergence behaviors observed for the Lorenz system in Section 2 and various numerical schemes of the viscous Burgers' equation in Section 3. Furthermore, Figure 15 highlights the recovered solution closely matches the

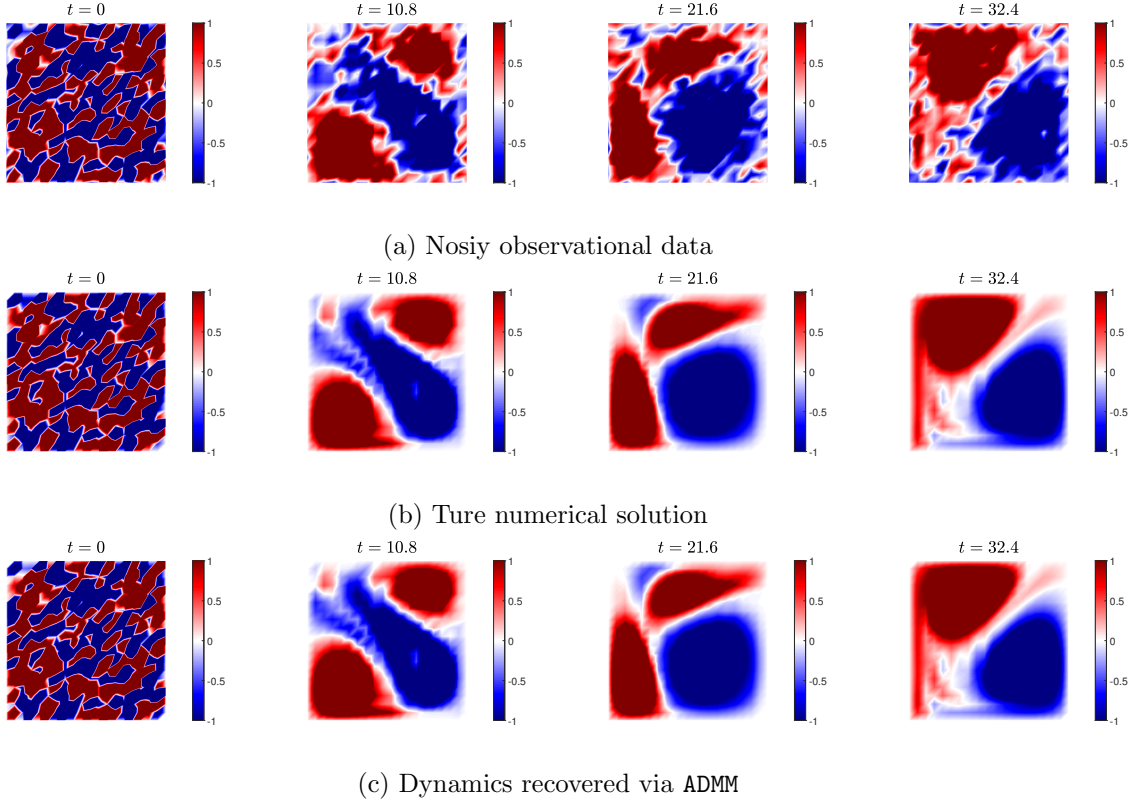


Figure 15: Comparison of noisy observational data with the time evolution dynamics recovered via the linearized multi-block ADMM with regularization (2.7), with the true numerical solution as the reference.

true dynamics, even in the presence of noisy observational data. The numerical errors, presented in Figure 16, further verify that the accuracy improves over time as the simulation progresses.

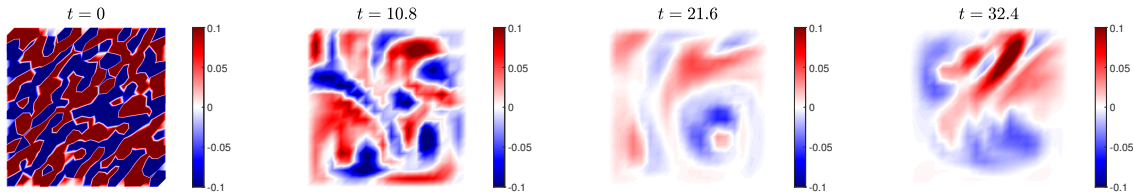


Figure 16: The error between the solution recovered via the linearized multi-block ADMM with regularization (2.7) and the true numerical solution.

By considering the scales of large-scale ocean circulation, with $L \sim 2.5\text{km}$ and vorticity $\omega_0 \sim 10^{-5}\text{s}^{-1}$, we derive a characteristic time scale of $\delta t \sim 7.2\text{h}$. With an iteration count of $N = 300$, the total simulation time becomes $T = N\delta t \approx 6$ years, allowing for a comprehensive characterization of the large-scale ocean circulation. Additionally, we note that a commonly used boundary condition is the periodic boundary condition [McWilliams, 1984], which necessitates the use of spectral methods rather than finite difference methods. The reason for this preference is that convergence using SOR and the conjugate gradient methods is typically poor due to the presence of a zero eigenvalue in the Laplacian operator.

5 Conclusions and future work

In this study, we propose a linearized multi-block ADMM with regularization to solve the 4D-Var problem, exploiting its separable structure. Unlike classical first-order optimization algorithms that primarily focus on initial conditions, our approach derives the Euler-Lagrange equation for the entire dynamical system, facilitating more effective use of observational data. When the initial condition is poorly chosen, the arg min operation steers the iteration towards the observational data, reducing sensitivity to the initial guess. The quadratic subproblems simplify the solution process, while the parallel structure enhances efficiency, particularly with modern computational resources. However, the computation of the adjoint operator remains a significant challenge, even in cases like 2D turbulence. Future research may explore addressing this issue using the sampling approach proposed by [Shi and Sun, 2023, Shi and Ma, 2024]. Additionally, stochastic gradient descent (SGD) and its variants, which have proven successful in deep neural networks [Shi et al., 2023, Shi, 2021], offer promising alternatives for solving 4D-Var problems. Another important direction for further research is the investigation of complex optimization problems [Sorber et al., 2012], as many governing equations, such as the nonlinear Schrödinger and Ginzburg-Landau equations, involve complex variables. Further theoretical and numerical studies, including the exploration of various numerical schemes, may provide valuable insights, especially in fields such as meteorology, oceanography, and climatology.

One of the key unresolved challenges is proving the convergence of the linearized multi-block ADMM with regularization and identifying the conditions under which this convergence occurs. Establishing convergence is essential, as it would confirm that the solution to the 4D-Var problem (1.5) is independent of numerical schemes, enabling a numerical realization for the implicit scheme. Additionally, for the analytic 4D-Var problem (1.3), the issue of uniqueness, particularly over longer time horizons, remains open, although it has been addressed for short intervals [Cox, 2015]. A promising future direction lies in developing infinite-dimensional ADMM-like iterations. In the case where $T = 0$, such an approach could lead to a novel method for constructing a solution to the governing differential equation. This method could draw inspiration from classical iterative techniques, such as Picard iteration and Newton iteration [Arnold, 1992], which have been successfully extended from finite to infinite dimensions. These ideas could also connect with advanced frameworks like KAM iteration [Kolmogorov, 1954, Arnold, 2009, Moser, 1962] and Nash-Moser iteration [Nash, 1956, Moser, 1966a,b], which have significant applications, including in Landau damping [Mouhot and Villani, 2011]. Further exploration of these concepts could deepen our understanding of ADMM in infinite-dimensional spaces.

Acknowledgements

Bowen Li was partially supported by the Hua Loo-Keng scholarship of CAS. Bin Shi was partially supported by Grant No.12241105 of NSFC.

References

- V. I. Arnold. *Ordinary differential equations*. Springer Science & Business Media, 1992.
- V. I. Arnold. Proof of a theorem of A. N. Kolmogorov on the invariance of quasi-periodic motions under small perturbations of the Hamiltonian. *Collected Works: Representations of Functions, Celestial Mechanics and KAM Theory, 1957–1965*, pages 267–294, 2009.
- M. Asch, M. Bocquet, and M. Nodet. *Data assimilation: methods, algorithms, and applications*. SIAM, 2016.
- F. Bouttier and P. Courtier. Data assimilation concepts and methods march 1999. *Meteorological training course lecture series. ECMWF*, 718:59, 2002.
- E. Burman and L. Oksanen. Data assimilation for the heat equation using stabilized finite element methods. *Numerische Mathematik*, 139:505–528, 2018.
- E. Burman, A. Feizmohammadi, and L. Oksanen. A finite element data assimilation method for the wave equation. *Mathematics of Computation*, 89(324):1681–1709, 2020.
- R. H. Byrd, P. Lu, J. Nocedal, and C. Zhu. A limited memory algorithm for bound constrained optimization. *SIAM Journal on scientific computing*, 16(5):1190–1208, 1995.
- G. Cox. (Non) Uniqueness of critical points in variational data assimilation. *Physica D: Nonlinear Phenomena*, 300:34–40, 2015.
- B. Cushman-Roisin and J.-M. Beckers. *Introduction to geophysical fluid dynamics: physical and numerical aspects*, volume 101 of *International Geophysics*. Academic press, 2nd edition, 2011.
- Y.-H. Dai and Y. Yuan. A nonlinear conjugate gradient method with a strong global convergence property. *SIAM Journal on optimization*, 10(1):177–182, 1999.
- W. Deng and W. Yin. On the global and linear convergence of the generalized alternating direction method of multipliers. *Journal of Scientific Computing*, 66:889–916, 2016.
- L. El Bourkhissi, I. Necoara, and P. Patrinos. Linearized ADMM for nonsmooth nonconvex optimization with nonlinear equality constraints. In *2023 62nd IEEE Conference on Decision and Control (CDC)*, pages 7312–7317. IEEE, 2023.
- R. Fletcher and C. M. Reeves. Function minimization by conjugate gradients. *The computer journal*, 7(2):149–154, 1964.
- D. Gabay and B. Mercier. A dual algorithm for the solution of nonlinear variational problems via finite element approximation. *Computers & mathematics with applications*, 2(1):17–40, 1976.
- R. Glowinski and A. Marroco. Sur l’approximation, par éléments finis d’ordre un, et la résolution, par pénalisation-dualité d’une classe de problèmes de dirichlet non linéaires. *Revue française d’automatique, informatique, recherche opérationnelle. Analyse numérique*, 9(R2):41–76, 1975.
- G. H. Golub and C. F. Van Loan. *Matrix computations*. Johns Hopkins University Press, 4th edition, 2013.

- B. He, L. Hou, and X. Yuan. On full Jacobian decomposition of the augmented Lagrangian method for separable convex programming. *SIAM Journal on Optimization*, 25(4):2274–2312, 2015.
- M. R. Hestenes and E. Stiefel. Methods of conjugate gradients for solving linear systems. *Journal of Research of the National Bureau of Standards*, 49(6), 1952.
- L. T. K. Hien and D. Papadimitriou. An inertial ADMM for a class of nonconvex composite optimization with nonlinear coupling constraints. *Journal of Global Optimization*, pages 1–22, 2024.
- E. Kalnay. *Atmospheric Modeling, Data Assimilation and Predictability*. Cambridge University Press, 2002.
- A. N. Kolmogorov. On the conservation of conditionally periodic motions under small perturbation of the hamiltonian. *Dokl. Akad. Nauk. SSSR.*, 98:527–530, 1954.
- K. Law, A. Stuart, and K. Zygalakis. Data assimilation: A mathematical introduction. *Cham, Switzerland: Springer*, 214:52, 2015.
- F.-X. Le Dimet and O. Talagrand. Variational algorithms for analysis and assimilation of meteorological observations: theoretical aspects. *Tellus A: Dynamic Meteorology and Oceanography*, 38(2):97–110, 1986.
- X. Li, X. He, W. Gong, and C. C. Douglas. Variational data assimilation with finite-element discretization for second-order parabolic interface equation. *IMA Journal of Numerical Analysis*, page drae010, 2024.
- J. L. Lions. *Optimal Control of Systems Governed by Partial Differential Equations*. Springer-Verlag, 1971.
- E. N. Lorenz. Deterministic nonperiodic flow. *Journal of atmospheric sciences*, 20(2):130–141, 1963.
- G. I. Marchuk. Formulation of the theory of perturbations for complicated models. *Applied Mathematics and Optimization*, 2(1):1–33, 1975a.
- G. I. Marchuk. Formulation of the theory of perturbations for complicated models, Part II: Weather prediction. *Geofisica International*, 15(2):169–182, 1975b.
- J. C. McWilliams. The emergence of isolated coherent vortices in turbulent flow. *Journal of Fluid Mechanics*, 146:21–43, 1984.
- J. Möser. On invariant curves of area-preserving mappings of an annulus. *Nachr. Akad. Wiss. Göttingen, II*, pages 1–20, 1962.
- J. Moser. A rapidly convergent iteration method and non-linear partial differential equations-I. *Annali della Scuola Normale Superiore di Pisa-Scienze Fisiche e Matematiche*, 20(2):265–315, 1966a.
- J. Moser. A rapidly convergent iteration method and non-linear partial differential equations-I. *Annali della Scuola Normale Superiore di Pisa-Scienze Fisiche e Matematiche*, 20(3):499–535, 1966b.
- C. Mouhot and C. Villani. On landau damping. *Acta Mathematica*, 207(1):29–201, 2011.
- W. H. Munk and C. I. Wunsch. Observing the ocean in the 1990s. *Philosophical Transactions of the Royal Society of London. Series A, Mathematical and Physical Sciences*, 307(1499):439–464, 1982.
- J. Nash. The imbedding problem for riemannian manifolds. *Annals of mathematics*, 63(1):20–63, 1956.
- J. Pedlosky. *Ocean circulation theory*. Springer Science & Business Media, 1996.
- E. Polak and G. Ribiere. Note sur la convergence de méthodes de directions conjuguées. *Revue française d’informatique et de recherche opérationnelle. Série rouge*, 3(R1):35–43, 1969.

- D. Sanz-Alonso, A. Stuart, and A. Taeb. *Inverse Problems and Data Assimilation*. London Mathematical Society Student Texts. Cambridge University Press, 2023.
- Y. Sasaki. An objective analysis based on the variational method. *Journal of the Meteorological Society of Japan. Ser. II*, 36(3):77–88, 1958.
- Y. Sasaki. Proposed inclusion of time. variation terms, observational and theoretical, in numerical variational objective analysis. *Journal of the Meteorological Society of Japan. Ser. II*, 47(2):115–124, 1969.
- Y. Sasaki. Some basic formalisms in numerical variational analysis. *Monthly Weather Review*, 98(12):875–883, 1970.
- B. Shi. On the hyperparameters in stochastic gradient descent with momentum. *arXiv preprint arXiv:2108.03947*, 2021. To appear in *Journal of Machine Learning Research*, 2024.
- B. Shi and J. Ma. The sampling method for optimal precursors of el niño–southern oscillation events. *Nonlinear Processes in Geophysics*, 31(1):165–174, 2024.
- B. Shi and G. Sun. An adjoint-free algorithm for conditional nonlinear optimal perturbations (cnops) via sampling. *Nonlinear Processes in Geophysics*, 30(3):263–276, 2023.
- B. Shi, W. Su, and M. I. Jordan. On learning rates and schrödinger operators. *Journal of Machine Learning Research*, 24(379):1–53, 2023.
- G. Siedler, S. M. Griffies, J. Gould, and J. A. Church. *Ocean circulation and climate: a 21st century perspective*. Academic Press, 2013.
- L. Sorber, M. V. Barel, and L. D. Lathauwer. Unconstrained optimization of real functions in complex variables. *SIAM Journal on Optimization*, 22(3):879–898, 2012.
- D. Stammer, M. Balmaseda, P. Heimbach, A. Köhl, and A. Weaver. Ocean data assimilation in support of climate applications: Status and perspectives. *Annual review of marine science*, 8(1):491–518, 2016.
- O. Talagrand. 4D-VAR: four-dimensional variational assimilation. In *Advanced Data Assimilation for Geosciences: Lecture Notes of the Les Houches School of Physics: Special Issue, June 2012*. Oxford University Press, 2014.
- O. Talagrand and P. Courtier. Variational assimilation of meteorological observations with the adjoint vorticity equation. Part I: Theory. *Quarterly Journal of the Royal Meteorological Society*, 113(478):1311–1328, 1987.
- P. D. Thompson. Reduction of analysis error through constraints of dynamical consistency. *Journal of Applied Meteorology (1962-1982)*, pages 738–742, 1969.
- C. Wunsch. *The Ocean Circulation Inverse Problem*. Cambridge University Press, 1996.
- C. Wunsch and P. Heimbach. Dynamically and kinematically consistent global ocean circulation and ice state estimates. In *International Geophysics*, volume 103, pages 553–579. Elsevier, 2013.
- Y. Xie and S. J. Wright. Complexity of proximal augmented lagrangian for nonconvex optimization with nonlinear equality constraints. *Journal of Scientific Computing*, 86:1–30, 2021.
- X. Zhang, M. Burger, X. Bresson, and S. Osher. Bregmanized nonlocal regularization for deconvolution and sparse reconstruction. *SIAM Journal on Imaging Sciences*, 3(3):253–276, 2010.
- C. Zhu, R. H. Byrd, P. Lu, and J. Nocedal. Algorithm 778: L-bfgs-b: Fortran subroutines for large-scale bound-constrained optimization. *ACM Transactions on mathematical software (TOMS)*, 23(4):550–560, 1997.